Journal of Materials Chemistry B

Accepted Manuscript

ROYAL SOCIETY OF CHEMISTRY

www.rsc.org/materialsB

Journal of Materials Chemistry B

PAPER

Fabrication of Biomimetic Bundled Gel Fibres Using Dynamic Microfluidic Gelation of Phase-Separated Polymer Solutions

Cite this: DOI: 10.1039/x0xx00000x

Received 00th January 2012,
Accepted 00th January 2012

DOI: 10.1039/x0xx00000x

www.rsc.org/MaterialsB

Young-Jin Kim,[‡,a,b] Yuta Takahashi,[‡,a,c] Norihiro Kato,[c] and Yukiko T. Matsunaga,[*,a,d]

Here, we discuss fabrication of biomimetic bundle-structured gel fibres using a microfluidic device and rapid cross-linking of a phase-separated polymer blend solution. The products are potential candidates for cell culture scaffolds that mimic artificial tissues. Two naturally derived, biocompatible polysaccharide polymers are the raw materials for the bundled gel fibres, which are approximately 200 ~ 400 μm in a diameter and consist of 10^2~10^4 aligned continuous microfibres at 1 ~ 3 μm in a diameter. They create a composite fibrous material with enhanced toughness and tensile strength because of the unique three-dimensional, cross-linked hierarchic structure. Because the main component of the gel fibre is temperature responsive, the mechanical properties improve at higher temperatures, yet are reversible without collapse in response to temperature changes. Cell cultures form a cylinder-like shape along the fibre orientation. These unique features would be advantageous for tissue scaffolds as well as other biomaterial applications such as tissue engineering, actuators, drug carriers, and biosensors with "on-off" remotely controllable properties.

1. Introduction

Fibrous structures have been widely developed with a diverse range of geometries, from simple fibres, core-shell structures, to yarns. They are used in filters, electronic devices, and in biomaterial.[1-6] In particular, bundles of thin, multiply parallel fibres are widely seen in nature such as plant matter, notably in xylems, and human protein assemblies and muscle tissue.[7-11] Moreover, this structure is particularly appropriate for artificial tissues because of their similarity to soft natural tissues, such as the extra cellular matrix, at both micrometer and nanometer length scales.[12, 13] Because of their hierarchical structure, they have superior toughness and strength relative to single fibres, and have been a key research focus in artificial tissue engineering.[14, 15] To construct artificial tissues *in vitro*, soft matter such as polymers, proteins, or colloids have been used because of the ease of fabrication and handling, as well as for the ability to design and manipulate complex, unique structures with two or more components.[16-19] Thus, biomimetic bundled fibrous structures of soft matter could be used for soft tissue engineering. But facile synthesis is still lacking.

Current approaches have been limited by the complexity of fabrication methods that require expensive equipment and specialized multiple-step techniques.[20, 21] However, recent advances in microfluidics have enabled the precise control of multiple fluids, particularly for generating hierarchical fibrous hydrogels.[22, 23] These devices enable facile and dynamically adjustable control of experimental parameters. Particularly noteworthy in the synthesis of fibrous materials is the ability to tune shear stress. This is because, under sheath-flow conditions, macromolecules tend to form aligned self-

[a]Institute of Industrial Science, The University of Tokyo, 4-6-1 Komaba, Meguro-ku, Tokyo, 153-8505, Japan.

[b]Japan Society for the Promotion of Science (JSPS), 8 Ichibancho, Chiyoda-ku, Tokyo, 102-8472, Japan.

[c]Graduate School of Engineering, Utsunomiya University, 7-1-2 Yoto, Utsunomiya, Tochigi, 321-8585, Japan.

[d]PRESTO, Japan Science and Technology Agency, 4-1-8 Honcho, Kawaguchi, Saitama, 332-0012, Japan.

‡These authors contributed equally.

*Address correspondence to mat@iis.u-tokyo.ac.jp

†Electronic Supplementary Information (ESI) available: Additional movies of results are included. See DOI: 10.1039/b000000x/

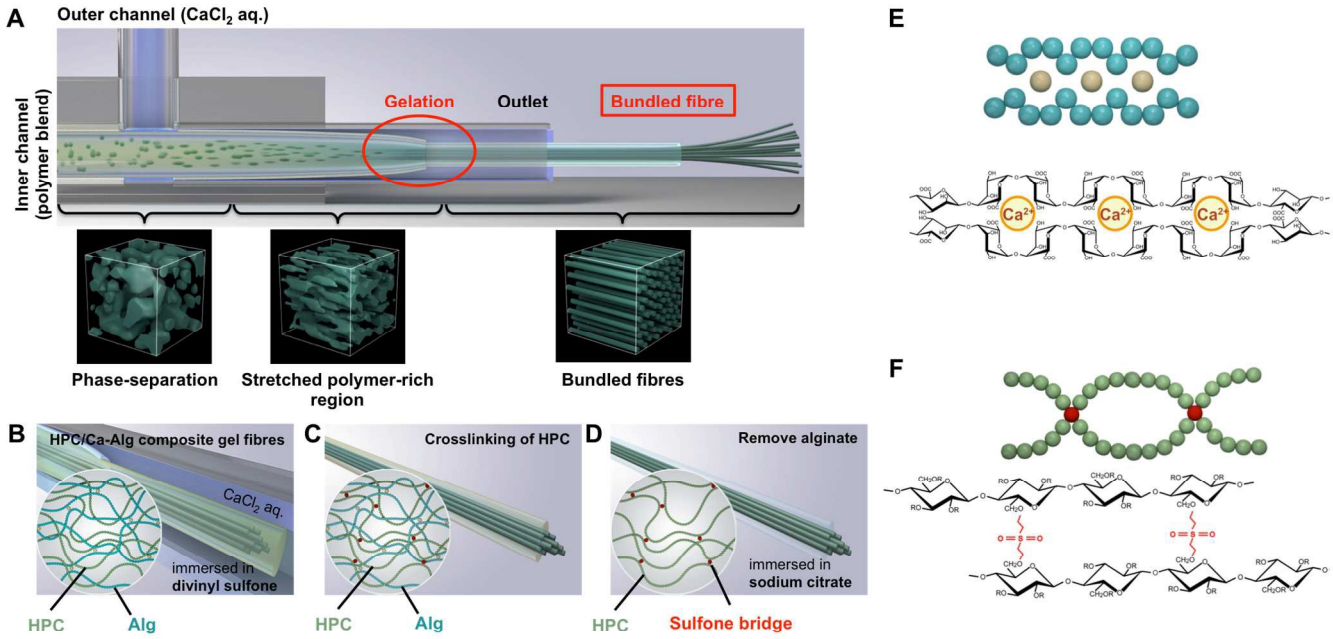

Figure 1. Concept of generating bundled gel fibres using a phase-separated polymer solution and a co-flow microfluidic device. (A) Polymer-rich regions in the phase-separated polymer solution are stretched by shear stress in the inner channel of a co-flow microfluidic capillary and transformed into bundles of gel fibres. (B) Na-Alg molecules in the gel fibres are immediately cross-linked by a $CaCl_2$ aqueous solution from an outer channel, *via* substitution of sodium ions in the G-residues of the alginate for Ca^{2+}. (C) After Na-Alg cross-linking, the whole structure is soaked in DVS aqueous solution to cross-link the HPC molecules. Stable bridges form *via* the reaction between DVS sulfone groups and HPC hydroxyl groups. (D) Finally, by removing un-reacted Na-Alg with citric acid, the stable HPC bundled gel fibre is obtained. (E) Structure of Ca-Alg cross-linked with Ca^{2+}. (F) Structure of HPC cross-linked with DVS.

assembled structures in a bottom-up process,[24] while phase-separated polymers have string-like structures from a top-down process[25].

Here, we discuss a method to generate in microfluidic channels bundled fibrous gel structures using a combination of sheath-flow and phase-separation of a polymer blend solution. Specifically, we generate bundled fibrous architectures from polymer-rich regions of an aqueous mixture of hydroxypropyl cellulose (HPC) and sodium alginate (Na-Alg). Our strategy is schematically depicted in Fig. 1. We used a co-flow microfluidic device allowing dynamic gelation of a polymer blend in a phase-separated state under shear stress (Fig. 1A). In this study, we introduce a 3-D simple PDMS-based glass capillary co-flow microfluidic device instead of 2-D lithography-based microfluidic device because our microfluidic device can reduce wetting phenomena[26, 27] that would be strongly influenced in flow of polymer blend solution, pattern of phase-separation and fibre morphology. Due to relatively rapid flow rate of low viscous solution ($CaCl_2$ aq. solution), high viscous solution (polymer blend aq. solution) can maintain the stable flow at outlet allows obtaining the well-defined parallel and continuous bundled gel fibre. The other advantages of our device compared to other devices, which are prepared by soft-lithography photolithography or 3D printer, are as follows: (i) we can rapidly fabricate long, continuous, and multiple three-dimensional fibrous gels in a single process; (ii) the method and product are eco-friendly; (iii) the procedure is simple and cost-effective. We used a mixture of two different biocompatible polysaccharide-based polymers as raw materials (HPC and Na-Alg) that can phase separate. To produce the fibres, the phase-separated polymer solution and the calcium chloride ($CaCl_2$) cross-linker for Na-Alg are respectively injected into the inner and outer channels of the co-flow microfluidic device. The polymer-rich domains in the phase-separated polymer solution in the inner channel are then elongated with neighbouring domains by shear stress driven by syringe pumping. The long, continuous, bundled gel fibres are then immediately cross-linked on contact with the calcium ions. Two Na^+ ions in gluronate (G)-residues of Na-Alg are substituted for Ca^{2+} to maintain the original, elongated structure of the HPC/Ca-Alg composite hydrogel fibres produced in the inner flow (Fig. 1B and C). Subsequently, sulfone bridges to HPC hydroxyl groups are formed by adding divinylsulfone (DVS) cross-linker (Fig. 1D and E). Finally, un-reacted Alg molecules are removed by adding citric acid (Fig. 1F).

2. Materials

Sodium alginate (Na-Alg) was kindly provided by Kimica Corporation (Tokyo, Japan). The HPC (average MW: 100 kDa) and divinyl sulfone (DVS) were obtained from Sigma-Aldrich (Tokyo, Japan) and Tokyo Chemical Industry (TCI, Tokyo, Japan), respectively. Calcium chloride ($CaCl_2$) and sodium

hydroxide (NaOH) were purchased from Kanto Chemicals (Tokyo, Japan). Citric acid was purchased from Nacalai Tesque, Inc. (Kyoto, Japan). SILPOT 184 (polydimethylsiloxane (PDMS)) and its catalyst SILPOT were purchased from Dow Corning Toray (Tokyo, Japan). Rhodamine B isothiocyanate (RITC) and fluorescein isothiocyanate (FITC) were purchased from Sigma-Aldrich (Tokyo, Japan). Ethylenediamine, sulfo-*N*-hydroxysuccinimide (sulfo-NHS), 1,6-diaminohexane and 1-ethyl-3-(3-dimethylaminopropyl)carbodiimide (EDC) were purchased from TCI (Tokyo, Japan). 1,1-Carbonyldiimidazole was obtained from Wako (Tokyo, Japan). All other chemicals and solvents were used as purchased. Distilled water from a Milli-Q system (Merck Millipore, Darmstadt, Germany) was used in all experiments.

3. Methods

3.1. Preparation of co-flow microfluidic device

The co-flow microfluidic device was fabricated using a slightly modified method reported previously by Kiriya et al.[28] As illustrated in Figs. S1 and S2, the device is consisting of a PDMS connector, glass capillaries and silicone tubes attached to the PDMS connector. Briefly, degassed liquid PDMS pre-polymer solution was cast onto the 10 mm petri dish where two C_2F_4 coated rectangle glass capillary tubes and the Tefzel® tube (ETFE) tubes are presented, and then cured for 5 hours at 75 °C (Fig. S1A). The cured PDMS and all tubes are disassembled, and then cut to the desired dimension (detail dimension is shown in Fig. S1B) before punching a hole through the PDMS for an inlet (for $CaCl_2$ aq. solution). The glass capillary channels are comprised of two types of glass capillaries and connectors. In brief, a round glass capillary tube (1 mm outer diameter, 0.6 mm inner diameter, G-1, Narishige, Tokyo, Japan) was stretched and tapered by a micropipette puller (PC-10, Narishige Co. Ltd, Tokyo, Japan) to a 300 µm diameter, then inserted into a rectangle glass tube (1.4 mm outer diameter, 1 × 1 mm inner dimensions, Vitrocom Inc., Mountain Lakes, NJ, USA). The rectangle glass tube was inserted into the PDMS mould and then round silicone tubes were inserted into two inlets as connectors. After assembly silicone tubes, the PDMS with microchannels was fixed on a slide glass after O_2 plasma treatment by plasma cleaner for 1 min (PDC-32C, Harrick Plasma, Ithaca, NY, USA) and then sealed all small gaps by curing PDMS pre-polymer solution (Fig. S2).

3.2. Synthesis of FITC-HPC

HPC (300 mg) was dissolved in 30 mL of dimethyl sulfoxide (DMSO) for 4 hours. 1,1-Carbonyldiimidazole (450 mg) was added to the solution and then stirred for 4 hours with N_2 gas bubbling. For amine termination, 1,6-diaminohexane was added and stirred for 24 hours. Amine-terminated HPC was obtained by dialysis and lyophilisation for 7 and 4 days, respectively. The amine-terminated HPC and the FITC (1.5 mg) were mixed in MilliQ water for 48 hours at 4 °C, then purified by dialysis and lyophilisation again for 7 and 4 days, respectively.

3.3. Synthesis of RITC-Alg

Na-Alg (500 mg) was dissolved in 0.1 M of sodium acetate buffer with EDC (150 mg) and sulfo-NHS (120 mg) and stirred for 6 hours to activate the carbonyl groups in Alg. Ethylenediamine was added and stirred for 2 days. The solution was then precipitated twice in 2-propanol to remove unreacted amine and precipitates were dried under vacuum over night. Amine-terminated Alg was dissolved in sodium bicarbonate buffer and stirred for 6 hours and then reacted with RITC (2 mg) for 2 days at 4 °C. Finally, RITC-Alg was purified by dialysis and lyophilisation for 7 and 4 days, respectively.

3.4. Characterisation of polymer solution

The pH of all polymer solutions was adjusted to 13 by adding 5 M NaOH. Phase transitions of all the solutions were investigated by transmittance with a UV-Vis spectrometer (JASCO International Co., Ltd., Tokyo, Japan), equipped with a Peltier temperature controller (10 ~ 50 °C). HPC (2.0 ~ 7.0 wt%) and Na-Alg (fixed at 1 wt%) polymer blend solutions were prepared by dissolving in Milli-Q water and stirring for 24 hours at pH 7 and 13. To obtain the microscope images for H5A1, polymer solutions at pH 7 and 13 were separately dropped onto a 3 mm-thick PDMS chamber, then covered with a coverslip. The solution was observed with phase-contrast microscopy (AxioObserver D1, Carl Zeiss, Oberkochen, Germany) at temperatures ranging from 15 to 45 °C. Polymer solutions of FITC-HPC (0.1 wt% of total amount of HPC) and RITC-Alg (0.1 wt% of total amount of Alg) were imaged with CLSM (LSM 700, Carl Zeiss, Oberkochen, Germany) at 28 °C using excitations at 488 nm for FITC and 568 nm RITC.

3.5. Fabrication of Alg gel fibre, HPC non-bundled gel fibre and HPC bundled gel fibre

For the fabrication of an Alg gel fibre as a control sample, we used an aqueous pre-gel solution of Na-Alg. Otherwise, the procedure was the same as that used for fabrication of bundled gel fibres. The Ca-Alg gel fibres were preserved in 0.1 M $CaCl_2$ aqueous solution at 4 °C.

HPC non-bundled gel fibres were fabricated from an HPC aqueous solution with pH adjusted to 13 by 5 M NaOH. It was then mixed with DVS as a cross-linker (1.1 wt%) and stirred at room temperature for 40 seconds. The HPC solution was injected into a silicone tube (0.5 mm inner diameter, 150 mm length) with a syringe. The tube was then immersed in Milli-Q water for 24 hours at 25 °C. HPC non-bundled gel fibres were then pulled out from the silicone tube.

To generate HPC bundled gel fibre, we used aqueous solutions of HPC and Na-Alg at 28 °C. A glass syringe filled with the solution was connected to the inner capillary channel along a silicone tube, and then placed on a syringe pump. Another syringe was connected to the outer capillary channel along a different silicone tube, and then placed on a second syringe pump containing $CaCl_2$ for Na-Alg cross-

linking. The flow rates were fixed at 300 µL/min and 2,500 µL/min for the polymer and $CaCl_2$ solutions, respectively. Simultaneous flow from both syringes produced the HPC/Ca-Alg bundled gel fibres. The fibres were immersed in DVS solution (2.0 wt%, pH 13) for HPC cross-linking for 12 hours under agitation (84 rpm). Citric acid was added to remove un-reacted Alg molecules. Numerical values and strain rate of the polymer blend solution within the microfluidic device are summarized in the Fig. S2C.

3.6. Characterisation of non-bundled gel fibres and bundled gel fibres

Images of gel and bundled gel fibres were obtained with a phase-contrast microscope, a dry state FE-SEM (SU8000, Hitachi, Tokyo, Japan) and a wet state SEM (QuantaTM 250 FEG electron microscope FEI, Hillsboro, OR, USA). For the dry state FE-SEM, the samples were lyophilised and coated with Pt for 60 seconds using a magnetron-sputter coater (MSP-1S, Vacuum Device Inc., Tokyo, Japan). The wet samples were used for the wet state SEM without further coating and lyophilisation.

A universal testing machine (UTM, EZ-SX, Shimadzu, Kyoto, Japan) was used to characterize the mechanical properties of the all gel fibres. Each specimen was placed so that the chuck-to-chuck spacing was 20 mm, and pulled at a 10 mm/min load cell rate at 25 °C in a humid environment. To evaluate shrinking and swelling ratio of bundled gel fibres at different temperature, the shrinkage stress caused by heating and cooling was measured by pulling the fibres by 0.5 mm. After 30 seconds, cycles of heating and cooling (heating: 64 °C, 5 min / cooling: 25 °C, 10 min) were repeated three times by applying hot water vapour.[29]

3.7. Cell culture experiments

HPC bundled gel fibres were initially coated with PLL-g-PEG-RGD for enhanced cell attachment. Suspended NHDFs (normal human dermal fibroblasts) in Dulbecco's modified Eagle's medium with 10% fetal bovine serum (FBS) and 1% antibiotics (AB) were seeded on the bundled gel fibres at 7,000 cell/mL, and incubated in a 5% CO_2 atmosphere at 37 °C. The culture medium was changed every 2 days. To confirm cell viability, the cells were incubated with Live/Dead® cytotoxicity/viability kit (Molecular Probe, Invitrogen, Carlsbad, CA, USA) and imaged with CLSM after 1 and 3 days. After 3 and 6 days, immunofluorescence images of F-actin and nuclei were also acquired. To this, the cells were fixed in 4% paraformaldehyde for 10 minutes, then the F-actin and the nuclei were respectively stained with Alexa568-conjugated phalloidin and Hoechst33342 (Molecular Probe, Invitrogen, Carlsbad, CA, USA). The stained cells were imaged with CLSM. Cell orientation angles were determined by immunostained images using Image J. The orientation angle of an individual cell was measured as the angle against the fibre direction.

4 Results

4.1. Preparation and characterisation of aqueous phase-separated polymer solution

To obtain the optimal phase-separated polymer solution, we investigated the phase-separation behaviour by controlling concentration, temperature and pH, all of which can strongly affect the process.[30, 31] We thus used a phase-contrast microscope to monitor the phase-separation of different HPC/Na-Alg ratios at different temperatures and pH values. (Note that different polymer mixtures are abbreviated as H*X*A*Y*, where "H" and "A" indicate HPC and Na-Alg, and "*X*" and "*Y*" indicate their respective concentrations in wt %. For example, H5A1 is a polymer solution of 5 wt% HPC and 1 wt% Na-Alg.) No polymer-rich domains and polymer networks were observed at pH 7, even when the solutions became turbid after heating above the lower critical solution temperature (LCST). Therefore, there is just a coil-globule transition (Fig. 2A top and Movie S1). In contrast, small polymer droplets were observed at 25 °C and pH 13, and their size gradually increased with temperature up to 45 °C. They consequently formed a polymer-rich network through the connection of the droplets (Fig. 2A bottom and Movie S2). This phase-separation was also observed with a CLSM by using FITC-HPC and RITC-Alg. There is a clear separation into polymer-rich and solvent-rich domains at 28 °C, and there is a co-existence of both HPC and Alg in the polymer-rich region (Fig. 2B, Movie S3). Furthermore, the polymer-rich region forms a three-dimensional, bi-continuous network structure (Movie S4).

To investigate the temperature dependence of the phase-separation, the blended polymer solutions were characterized with UV-Vis spectroscopy where they exhibited discontinuous transmittance changes in a distinctly narrow temperature range (Fig. S3). The cloud point of the solution containing only HPC at pH 7 was at 43 °C, and decreased to 37 °C with the addition of 1 wt% of Na-Alg (Fig. 2C and Fig. S3A). The latter occurs because the dissociated salt ions from Na-Alg reduce the water solubility of HPC *via* a salting-out effect,[32, 33] consequently shifting the cloud point to a lower temperature independent of the HPC concentration. This was also observed when NaOH was added to adjust the pH to 13; consequently, the cloud points decreased in pH 13 solutions (Fig. 2C and Fig. S3B). Furthermore, a two-step transmittance change was observed for pH 13 (Fig. 2D and Fig. S3C). (In Fig. 2C and D, we denote the lower transition temperature by $T_{phase\text{-}separation}$ and the higher transition point by $T_{coil\text{-}globule}$ on the transmittance curve, as indicated by arrows.) The first transmittance change in the phase-separated blend solutions indicates an initial phase-separation to polymer-rich and polymer-poor domains, because the reduced solubility of polymers accelerated the phase separation. The second transmittance change indicates a coil-globule transition of the HPC in the polymer-rich domains, which is characteristic of the temperature-responsive HPC. This was not observed for the polymer blend solutions at pH 7, which indicates no phase separations because dissociated salt ions from Na-Alg do not effect polymer phase separation (there is only a coil-globule transition). This is confirmed by comparing H5A0 and H5A1 solutions at pH 7 and 13. All the cloud points in each solution at both pH 7 and 13 are summarized in Fig. 2E. $T_{coil\text{-}globule}$ appears between 35 and 38 °C, which is almost identical to the LCSTs for H5A1 at pH 7, while $T_{phase\text{-}separation}$ is lower than 27 °C. These results are entirely consistent with the phase-contrast microscopy images shown in Fig. 2A. The

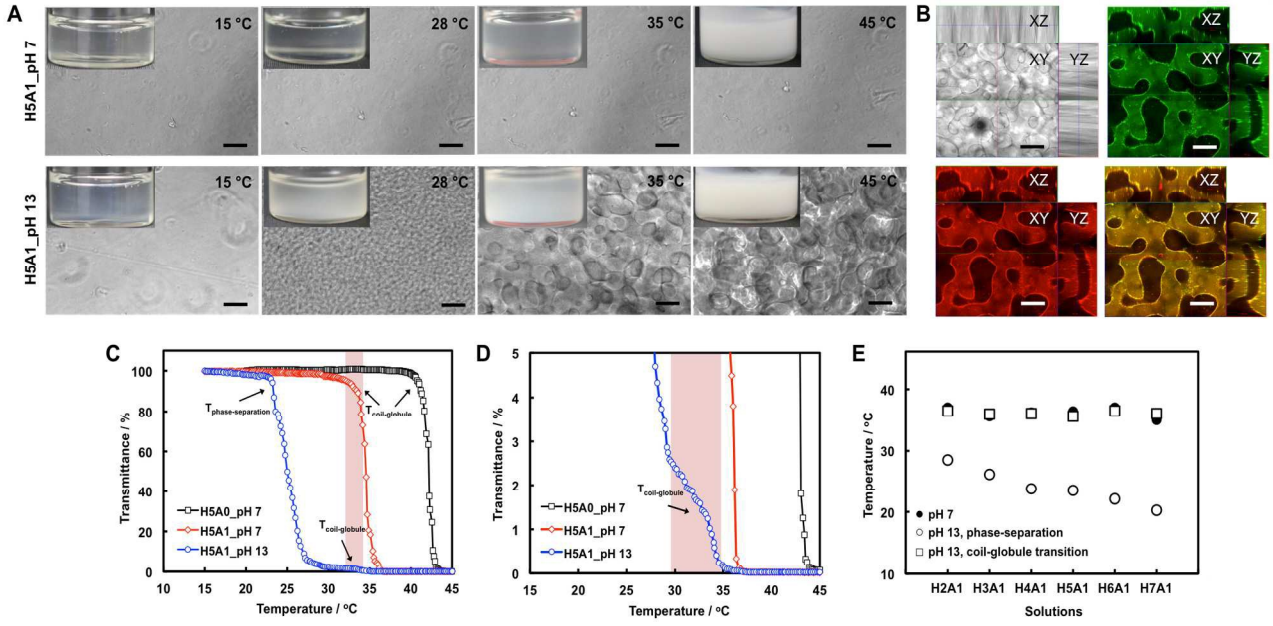

Figure 2. Properties of phase-separated polymer blend solutions at different temperatures and pH values. (A) Temperature-dependent changes (15 to 45 °C) in a H5A1 solution at pH 7 (top) and pH 13 (bottom). At pH 7 (top), no droplets were observed, even when the turbidity of the solution changed (insert images, over 35 °C). Whereas, at pH 13 (bottom), phase-separation occurs at 28 °C and droplets (polymer-rich region) gradually grow to form a network of polymer-rich regions. All scale bars are 100 µm. (B) CLSM images of H5A1 phase-separated solution (0.1% of FITC-conjugated HPC and RITC-conjugated Alg, pH 13, 28 °C). FITC-HPC (green), RITC-Alg (red), and merged (yellow) are shown. The HPC and Alg co-exist in a phase-separated polymer-rich region that forms a network structure. All scale bars are 500 µm. (C) ~ (E) Solution transitions investigated with UV-Vis spectroscopy for increasing temperature and different pH values. The H5A1 solution has a much lower phase transition temperature than does the HPC only solution at pH 7 because of a salt-out effect by Na^+ ion dissociation from Na-Alg. By changing the pH value from 7 to 13 with NaOH, the H5A1 solution now has two cloud points (arrows: one is phase-separation and the other is coil-globule transition), which are observed in (C) and (D) (blue circle). Cloud points of the solutions are summarized in (E).

H5A1 solution at pH 7 and near the LCST exhibited only a coil-globule phase transition without droplets or particles. At pH 13, however, there was a phase separation below LCST; subsequently, a coil-globule phase transition in the polymer-rich region was observed near the LCST of HPC. Given these unique properties, the H5A1 solution was used as a pre-gel solution because the production of bundles under flow relies on the polymer being initially isolated in polymer-rich regions that can subsequently elongate.

4.2. Generation of bundled gel fibres and their morphologies

We generated bundled gel fibres with the co-flow microfluidic device at 28 °C. The aqueous HPC/Na-Alg polymer blend solution and the aqueous $CaCl_2$ solution were injected respectively into the inner and outer channels at respective flow speeds of 300 µL/min and 2,500 µL/min. As shown in Fig. 3A and Movie S5, the phase-separated polymer networks (Fig. 3A-i) of the H5A1 at pH 13 in the inner channel were stretched by applying shear stress (Fig. 3A-ii), and were immediately fixed by cross-linking Alg with calcium ions (Fig. 3A-iii) in the co-flow region. We thus obtained bundled gel f ibres and non-bundled gel fibres with long lengths and extremely high aspect ratios (Fig. 3B). These features were made permanent by first soaking them in DVS solution to permanently cross-link the HPC molecules. Then bundled gel fibres were obtained by adding citric acid to remove the un-reacted Alg (Fig. 3C). Random disassembly of the fibrous structure was possible by using tweezers (Fig. 3D and Movie S6). The fibre bundles were 200 ~ 400 µm in a diameter and consisted of approximately 10^2 ~ 10^4 small fibres that were 1 ~ 3 µm in a diameter. Fabrication of the gel fibre bundles requires a phase-separated solution. Thus, no bundled fibres were obtained when using the non-phase-separated polymer blend solution at pH 7 (Fig. S4). Even at pH 13, no bundled structures were obtained with H2A1 and H3A1 blend solutions. Higher concentrations of HPC (H4A1, H5A1, H6A1 and H7A1), however, where phase separation is observed, yielded structures (Fig. S5). These results clearly demonstrate that the phase-separated state of the polymer blend, consisting of polymer-rich and polymer-poor regions, is a key prerequisite for bundle formation.

Detailed morphologies of fibres were imaged with SEM in both dry and wet states. In bundled fibres, many small non-porous fibres were observed, even after lyophilisation (Fig. 3E and Fig. S6A). The fibrous structures of the bundled gels in the wet state were also observed with SEM (Fig. S6B). Whereas, layered and porous morphologies were observed in pure Alg and HPC gel fibres, respectively. This is analogous to the morphological characteristics of common bulk hydrogels (Fig. S6C and D).

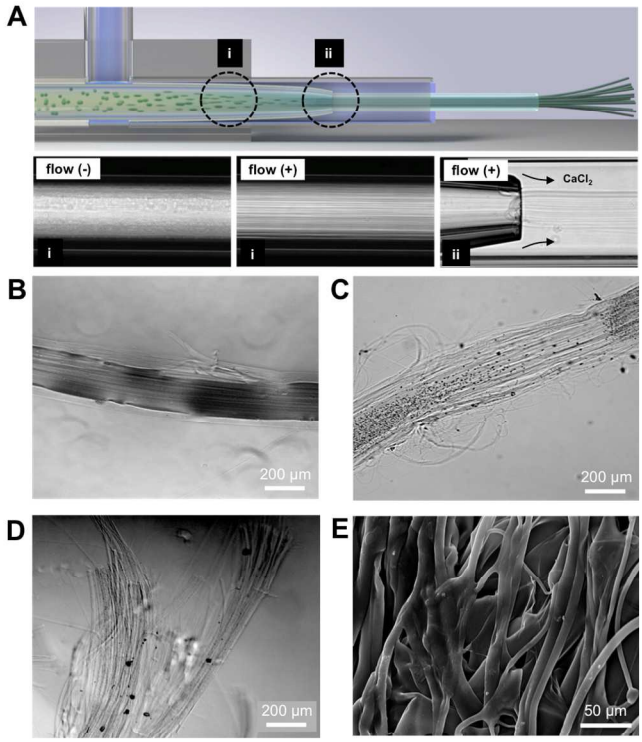

Figure 3. Generation of bundled gel fibres from the polymer blend solution (H5A1, pH13). (A) Optical microscope images of the polymer blend solution in the co-flow microfluidic device with and without flow condition at 28 °C. (B) Phase-contrast microscope images of bundled gel fibres (H5A1, pH13) after treatment with DVS. (C) and (D) Phase-contrast microscopic images of bundled gel fibres after removing Ca-Alg with citric acid. (E) SEM images of bundled gel fibre observed under wet conditions. The bundled gel fibres are approximately 200 ~ 400 μm in a diameter, and consist of many 1 ~ 3 μm diameter of microfibres.

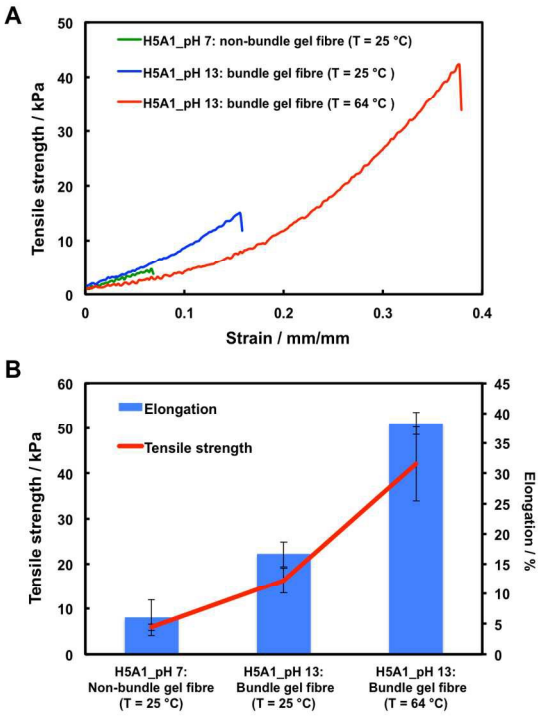

Figure 4. Mechanical strengths of non-bundled and bundled gel fibres measured at different temperatures with a UTM. The bundled gel fibre has much higher strength because of its dense structure. The bundled gel fibres became even stronger by dehydration and shrinking of HPC by increased temperatures.

4.3. Mechanical and "on-off' switchable properties of bundled gel fibre

We investigated the mechanical properties of the bundled gel fibres with a te nsile tester, as shown in Fig. 4. The tensile strength and elongation of the non-bundled gel fibres (H5A1 at pH7) and the bundled gel fibres (H5A1 at pH 13) were 5.9 ± 0.7 kPa, 6.0 ± 2.9%, 16.3 ± 2.9 kPa, and 16.6 ± 2.0%, respectively. These results can be understood by the structure of bundled gel fibres, which can disperse tensile forces among all the constituent small parallel fibres, and inhibit fibre breakage.[11] Furthermore, because the bundled gel fibres were fabricated from cross-linking concentrated polymer domains after phase separation, they have a higher polymer density and enhanced entanglement than do normal gel fibres after gelation. By increasing the temperature above the LCST, the tensile strength can be increased further (42.1 ± 8.2 kPa) because of the strong entanglements in HPC molecules induced by dehydration and shrinking. There was also a much greater elongation (38.3 ± 1.9%) than that observed for temperatures lower than the LCST. Tensile strength and elongation are generally inversely related.[34, 35] However, they both increased with temperature because the residual cross-linked Alg molecules deep in the bundled gel fibres contributed to the elongation instead of condensed HPC molecules above the LCST.

We also found "on-off" reversible changes in the strain of the bundled gel fibres in response to temperature oscillations around the LCST (Fig. 5A).[36] The gaps in the changing strain are almost a constant 3.5 mN during three temperature alternation cycles. The transparency of the fibres was also changed by hydration and dehydration, as shown in the Fig. 5B inserts. The average shrinking ratios were 37 ± 1% for the long axis and 15 ± 4.4% for the short axis (Fig. 5C).

4.3. Cell culturing on bundled gel fibres

The bundled gel fibres were used as a substrate for culturing NHDFs. After 3 days of cultivation, most of cells were still alive (Fig. S7). By immunostaining, we confirmed actin stress fibres in the cells after 3 (Fig. 6A) and 6 days (Fig. 6B) of cultivation. The cells did

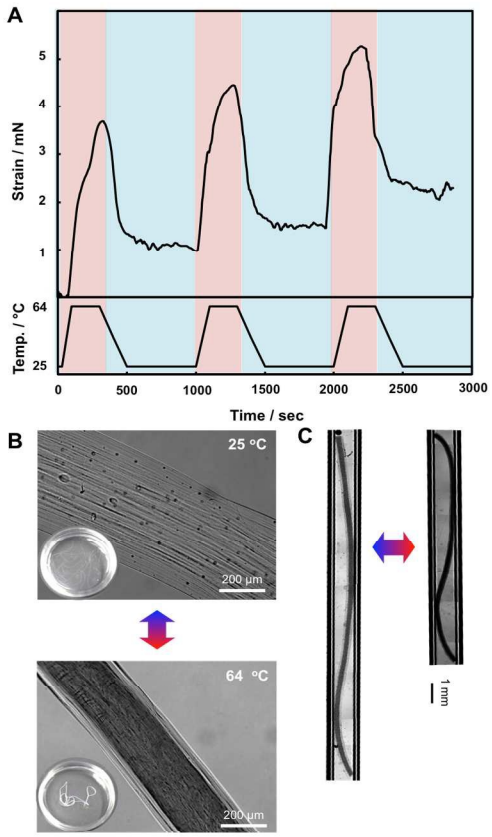

Figure 5. Changes in the mechanical properties and morphologies of bundled gel fibres with temperature oscillations between 25 and 64 °C. (A) Mechanical properties of the bundled gel fibres were reversible through three temperature cycles. The 3.5 mN steps in tension in each cycle were almost constant. (B) and (C) Temperature-dependent volume change of the bundled gel fibres because of HPC hydration-dehydration with temperature. The transparency and size of the bundled gel fibres were reversibly changed. The shrinkage ratio calculated from macroscopic images was 37 ± 1.0% for the long axis and 15 ± 4.4% for the short axis.

not fully cover the surface of the bundled gel fibre after 3 days of culturing. However, after 6 days, the fibres were fully covered with cells that expressed actin stress fibres. Most of the cells were aligned parallel to the micro fibres, forming a cylinder-like structure along the fibre bundle. In contrast, no cell orientation was observed on non-bundled gel fibre surfaces; instead they were randomly spread (Fig. 6C). The cell orientation angles are summarized in Fig. 6D.

5. Discussion

Phase-separation is commonly observed in blends of two-types or more polymers, which is useful for fabrication of porous or fibrous biomimetic matrices such as foams, sponges, and fibres.[37, 38] Our approach, however, fabricates biomimetic bundled gel fibre structure from a phase-separated polymer blend with a co-flow microfluidic device and shear stress.

HPC was selected as the primary material for the gel fibres because it is (i) thermo-sensitive, (ii) easy to acquire in various molecular weights, and (iii) biocompatible.[3, 9, 40] In particular, HPC has a LCST at 45 °C in aqueous solution and thus undergoes a reversible hydrated-to-dehydrated phase-transition with temperature increase. In this study, the phase-separated polymer blend of HPC with Na-Alg is rapidly cross-linked with Ca^{2+}, and maintains the string-like structure of the phase-separated solution formed by shear stress. The key point for phase-separation behaviour, in this study, is a concentration of salt in polymer blend aqueous solution. By adding slats (here, Na-Alg and NaOH), the dissociated Na^{+} ions can take much water molecules by attraction forces from polymer blend aqueous solution, which is called "salting-out effect".[33, 41] As a result, water solubility of polymers is reduced in aqueous system that leads to stronger interaction with polymer-polymer than polymer-water. Therefore, the homogenous polymer solution is separated into two phases (polymer-rich and -poor region) even at room temperature, which is lower than LCST of HPC. This phase-separation behaviour strongly depends on the concentration of salt ions. Consequently, the polymer blend solution exhibits: (i) an isotropic phase below 25 °C; (ii) an initial formation of droplets *via* spinodal decomposition at 25 °C; and (iii) droplet growth and network formation above 28 °C. These results demonstrate that the phase-separated state of polymer-rich and polymer-poor regions is key to bundle formation.

Phase-separated polymer solution can be stretched under the shear stress, then forming bundled fibre structures. In the present device, the major strain of the polymer flow occurs at the tapered junction point, and the radius of the inner channel and the tapered region determines the structures of the fibre elongation. As illustrated in the Fig. S2C, in the co-flow device, the polymeric flow in the inner channel experiences different strains at different locations: region 1 and region 2. Since the viscosity of the polymer solution (= 430 cP) is quite large, and therefore the Reynolds number is low, the polymeric flow in the inner channel is assumed to be laminar. The velocity profile across the inner channel at region 1 can be considered as a parabolic profile, and the strain rate becomes maximum value at the channel wall and linearly falls down to zero at the centre of the microchannel. On the other hand, the polymeric flow at the region 2 is accelerated at the tapered junction point, and the polymeric solution experiences stretching in the axial direction. Both the strain rate and the shear stress within the tapered region are estimated around 67 [s^{-1}] and 29 [Pa], respectively. Finally, after the tapered junction, the outer flow imposes force to the polymeric flow. However, since the viscosity of the polymer solution (=430 cP) is more than 400 times larger than that of the outer fluid, the polymer solution behaves like a solid and therefore dynamical effects of the outer flow can be neglected.

The bundled gel fibre was an effective scaffold for NHDFs cultures. While spreading along the bundled fibre, the cells

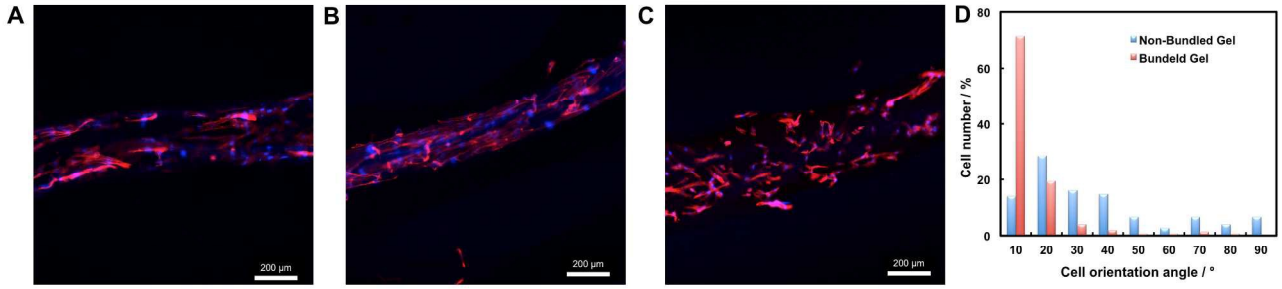

Figure 6. Immunostained NHDFs after culturing on bundled gel fibres for 3 days (A) and 6 days (B), respectively. F-actin stress fibre and nuclei were stained with rhodamine-phalloidin (red) and DAPI (blue) in fluorescence images. (C) NHDFs on non-bundled gel fibres after 6 days of cultivation. (D) Cell orientation angles on bundled gel fibres (red bar) and non-bundled gel fibres (blue bar). Cell orientation angles were measured using immunostained images of 6 days cultured cells.

fully covered the surface and formed a cylinder-like structure with cell orientations that mimicked vascular, muscle, tendon, and nerve tissues. Given its unique properties, such temperature-responsive property, biocompatibility and ease of manipulation near room temperature, HPC and its blends with the other polymers is an excellent candidate for soft tissue engineering. It is a unique scaffold because it has reversible mechanical properties that maintain the original structure in response to temperature oscillations. It could be a smart material with "on-off" switchable properties, remotely controllable, or be programmed according to the circadian rhythm of the body for transplant materials.[1, 29, 36]

6. Conclusions

We demonstrated a novel approach for preparing biomimetic bundled gel fibres using a dynamic microfluidic gelation system. The bundled gel fibres were fabricated by gelation of a phase-separated, temperature-responsive HPC polymer, derived from a natural polysaccharide, with a simple co-flow microfluidic device. By adjusting the pH of the H5A1 solution to 13, $T_{phase\text{-}separation}$ appeared near 25 °C. Phase separation was also directly observed *via* phase-contrast microscopy at the same temperature. Polymer-rich regions were transformed into bundled gel fibres by applying shear stress in the microfluidic channel. After subsequent cross-linking and dissolution of the alginate, stable and biomimetic bundled gel fibres were successfully obtained. They exhibited reversible thermo-responsive dimensions, transparencies, and mechanical properties. Furthermore, NHDFs cultured on the bundled gel fibres formed a cylinder-like shape similar to oriented cells in cylindrical tissues. Based on these results, these structures are excellent candidates for soft-tissue engineering of ligaments, muscles, veins, tendons or neuronal scaffolds, all of which require uniformly aligned, bundled fibrous scaffolds. Moreover, functionalisation of these structures with remotely switchable "on-off" properties, in addition to functionalisation with peptides, growth factors, or antibodies, can enable further applications such as filtration, sensing, and purification. Thus, further work with this exciting new material promises valuable returns.

Acknowledgements

This work was partly supported by PRESTO, Japan Science and Technology (JST), Japan. This work was also supported by a JSPS Grant-in-Aid for Young Scientists (A) (No. 25706010 to Y.T.M.).

References

1. Y.-J. Kim, M. Ebara and T. Aoyagi, *Adv. Funct. Mater.*, 2013, **23**, 5753-5761.
2. A. Greiner and J. H. Wendorff, *Angew. Chem. Int. Ed.*, 2007, **46**, 5670-5703.
3. E. Kang, Y. Y. Choi, S.-K. Chae, J.-H. Moon, J.-Y. Chang and S.-H. Lee, *Adv. Mater.*, 2012, **24**, 4271-4277.
4. S.-K. Chae, E. Kang, A. Khademhosseini and S.-H. Lee, *Adv. Mater.*, 2013, **25**, 3071-3078.
5. Y. Fu, X. Cai, H. Wu, Z. Lv, S. Hou, M. Peng, X. Yu and D. Zou, *Adv. Mater.*, 2012, **24**, 5713-5718.
6. D. Zhang, M. Miao, H. Niu and Z. Wei, *ACS Nano*, 2014, **8**, 4571-4579.
7. F. Liu, M. Prehm, X. Zeng, C. Tschierske and G. Ungar, *JACS*, 2014, **136**, 6846-6849.
8. A. R. Gillies and R. L. Lieber, *Muscle Nerve*, 2011, **44**, 318-331.
9. M. C. Ledbetter and K. R. Porter, *J. Cell Biol.*, 1963, **19**, 239-250.
10. C. E. Schafmeister, S. L. LaPorte, L. J. W. Miercke and R. M. Stroud, *Nat. Struct. Mol. Biol.*, 1997, **4**, 1039-1046.
11. S. Zhai, D. Li, B. Pan, J. Sugiyama and T. Itoh, *J Mater Sci*, 2012, **47**, 949-959.
12. T. Liedl, B. Hogberg, J. Tytell, D. E. Ingber and W. M. Shih, *Nat. Nanotechnol.*, 2010, **5**, 520-524.
13. M. Fang, E. L. Goldstein, A. S. Turner, C. M. Les, B. G. Orr, G. J. Fisher, K. B. Welch, E. D. Rothman and M. M. Banaszak Holl, *ACS Nano*, 2012, **6**, 9503-9514.

14. W.-Y. Lee, W.-Y. Cheng, Y.-C. Yeh, C.-H. Lai, S.-M. Hwang, C.-W. Hsiao, C.-W. Huang, M.-C. Chen and H.-W. Sung, *Tissue Eng. Pt. C: Meth.*, 2011, **17**, 651-661.
15. J. G. Barber, A. M. Handorf, T. J. Allee and W.-J. Li, *Tissue Eng. Pt. A*, 2011, **19**, 1265-1274.
16. D. Gonzalez-Rodriguez, K. Guevorkian, S. Douezan and F. Brochard-Wyart, *Science*, 2012, **338**, 910-917.
17. J.-Y. Sun, X. Zhao, W. R. K. Illeperuma, O. Chaudhuri, K. H. Oh, D. J. Mooney, J. J. Vlassak and Z. Suo, *Nature*, 2012, **489**, 133-136.
18. J. P. Gong, Y. Katsuyama, T. Kurokawa and Y. Osada, *Adv. Mater.*, 2003, **15**, 1155-1158.
19. Y. T. Matsunaga, Y. Morimoto and S. Takeuchi, *Adv. Mater.*, 2011, **23**, H90-H94.
20. U. Ali, Y. Zhou, X. Wang and T. Lin, *J. Text. I.*, 2011, **103**, 80-88.
21. W. E. Teo and S. Ramakrishna, *Nanotechnology*, 2005, **16**, 1878.
22. H. Onoe, T. Okitsu, A. Itou, M. Kato-Negishi, R. Gojo, D. Kiriya, K. Sato, S. Miura, S. Iwanaga, K. Kuribayashi-Shigetomi, Y. T. Matsunaga, Y. Shimoyama and S. Takeuchi, *Nat Mater*, 2013, **12**, 584-590.
23. B. G. Chung, K.-H. Lee, A. Khademhosseini and S.-H. Lee, *Lab Chip*, 2012, **12**, 45-59.
24. S. Köster, J. B. Leach, B. Struth, T. Pfohl and J. Y. Wong, *Langmuir*, 2006, **23**, 357-359.
25. T. Hashimoto, K. Matsuzaka, E. Moses and A. Onuki, *Phys. Rev. Lett.*, 1995, **74**, 126-129.
26. K. Tsougeni, D. Papageorgiou, A. Tserepi and E. Gogolides, *Lab Chip*, 2010, **10**, 462-469.
27. J. H. Xu, G. S. Luo, S. W. Li and G. G. Chen, *Lab Chip*, 2006, **6**, 131-136.
28. D. Kiriya, R. Kawano, H. Onoe and S. Takeuchi, *Angew. Chem. Int. Ed.*, 2012, **51**, 7942-7947.
29. Y.-J. Kim, M. Ebara and T. Aoyagi, *Sci. Tech. Adv. Mater.*, 2012, **13**, 064203.
30. H. Tanaka, *J. Phys.: Condens. Matter*, 2000, **12**, R207.
31. P. van de Witte, P. J. Dijkstra, J. W. A. van den Berg and J. Feijen, *J. Membr. Sci.*, 1996, **117**, 1-31.
32. H. Du, R. Wickramasinghe and X. Qian, *J. Phys. Chem. B*, 2010, **114**, 16594-16604.
33. M. J. Hey, D. P. Jackson and H. Yan, *Polymer*, 2005, **46**, 2567-2572.
34. K. Boustany and R. L. Arnold, *J. Elastomers Plast.*, 1976, **8**, 160-176.
35. C. Caner, P. J. Vergano and J. L. Wiles, *J. Food Sci.*, 1998, **63**, 1049-1053.
36. Y.-J. Kim, M. Ebara and T. Aoyagi, *Angew. Chem. Int. Ed.*, 2012, **124**, 10689-10693.
37. J. M. Holzwarth and P. X. Ma, *J. Mater. Chem.*, 2011, **21**, 10243-10251.
38. J. M. Holzwarth and P. X. Ma, *Biomaterials*, 2011, **32**, 9622-9629.
39. C. Chang and L. Zhang, *Carbohydr. Polym.*, 2011, **84**, 40-53.
40. Z. Yue, F. Wen, S. Gao, M. Y. Ang, P. K. Pallathadka, L. Liu and H. Yu, *Biomaterials*, 2010, **31**, 8141-8152.
41. R. Sadeghi and B. Jamehbozorg, *Fluid Phase Equilib.*, 2009, **280**, 68-75.